ARTICLE

Electron Momentum Spectroscopy of Valence Orbitals of n-Propyl Iodide: Spin-Orbit Coupling Effect and Intramolecular Orbital Interaction

En-liang Wang[a,b*], Yu-feng Shi[a,b], Xu Shan[a,b*], Hong-jiang Yang[a,b], Wei Zhang[a,b], Xiang-jun Chen[a,b]

a. Hefei National Laboratory for Physical Sciences at the Microscale and Department of Modern Physics, University of Science and Technology of China, Hefei 230026, China
b. Synergetic Innovation Center of Quantum Information and Quantum Physics, University of Science and Technology of China, Hefei 230026, China

(Dated: Received on May 3, 2014; Accepted on May 15, 2014)

The binding energy spectrum and electron momentum distributions for the outer valence orbitals of n-propyl iodide molecule have been measured using the electron momentum spectrometer employing non-coplanar asymmetric geometry at impact energy of 2.5 keV plus binding energy. The ionization bands have been assigned in detail via the high accuracy SAC-CI general-R method calculation and the experimental momentum profiles are compared with the theoretical ones calculated by Hartree-Fock and B3LYP/aug-cc-pVTZ(C,H)6-311G**(I). The spin-orbit coupling effect and intramolecular orbital interaction have been analyzed for the outermost two bands, which are assigned to the iodine 5p lone pairs, using NBO method and non-relativistic as well as relativistic calculations. It is found that both of the interactions will lead to the observed differences in electron momentum distributions. The experimental results agree with the relativistic theoretical momentum profiles, indicating that the spin-orbit coupling effect dominates in n-propyl iodide molecule.

Key words: n-Propyl iodide, Electron momentum spectroscopy, Spin-orbit coupling effect, Intramolecular orbital interaction

I. INTRODUCTION

Electron momentum spectroscopy (EMS) has been developed as a powerful tool for investigating the electronic structures of atoms and molecules since the pioneering works of McCarthy, Weigold and co-workers some forty years ago [1−4]. Two categories of information can be obtained by EMS: (i) binding energy spectra (BES) over a wide energy range usually covering the complete valence shell, and (ii) the angular distributions of (e, 2e) cross section for individual transitions giving rise to the peaks in BES. Within a series of approximations including binary encounter approximation, weak coupling approximation, plane wave impulse approximation and target Hartree-Fock (HF) or target Kohn-Sham (KS) approximation [5], the measured (e, 2e) cross section is proportional to the spherically averaged electron momentum distribution or electron momentum profile for a specific molecular orbital (MO).

During the last decades, EMS has been employed to extensively investigate the intramolecular orbital (IMO) interactions [6−8] and the related conformational effect for structurally versatile molecules such as glycine [9], n-butane [10], 1,3-butadiene [11], dimethoxymethane [12], 1-butene [13], tetrahydrofurane [14], ethanethiol [15], ethanol [8, 16], or ethylamine [17]. EMS has also been used to explore the spin-orbit (SO) coupling effects on the electronic structure of atoms [18, 19] and more recently on that of molecules [20−22].

SO coupling and IMO interaction are two competitive interactions within a molecule. They can co-exist in one single molecule like halogenated alkanes. For halogenated alkane molecules, the highest-occupied molecular orbitals (HOMOs) are usually formed by the non-bonding lone pair electrons of halogen atoms X (X=F, Cl, Br, I). The IMO interaction between lone pair orbitals (n) of halogen atom and other moieties of the molecule is the origin of the delocalization of halogen atomic lone pair electrons that leads to two different MOs. On the other hand, the SO coupling effect, which results from the interaction between the spin and orbital angular momenta of the halogen lone pair electrons, will cause the energy levels to split.

SO coupling effect and IMO interaction have most commonly been investigated by the high resolution photoelectron spectra (PES) [23−25]. If the IMO interaction is weak, for a halogenated alkane molecule of low symmetry (C_s symmetry), the two lone pair orbitals will energetically degenerate and can be approximated as one. Due to the SO coupling effect, the ionic term is split into two levels $^2E_{3/2}$ and $^2E_{1/2}$, and the twoioniza-

*Authors to whom correspondence should be addressed. E-mail: elwang@ustc.edu.cn, xshan@ustc.edu.cn

tion bands will be observed in PES. The space of band split will have full value of the SO interaction parameter of the relevant halogen atoms [26]. If, on the other hand, the IMO interaction is comparable to the SO coupling effect, the SO split bands of lone pair orbitals in PES can also be assigned using normal symmetries of MOs. In this situation, two split bands will overlap seriously, due to the delocalization of MO electrons. The two SO split bands will also show the vibrational fine structures due to their MO characters [26]. Halogenated alkanes have received continuous interest from Novak and coworkers [25]. In their work, the IMO interactions were studied by the photoelectron spectroscopy utilizing He I and He II as well as synchrotron radiation.

Besides the band split, SO coupling effect and IMO interaction can also lead to the change of the electron density distributions [27−29]. By measuring the collision energy dependence of partial ionization cross section (CEDPICS) employing Penning ionization electron spectra (PIES) [30−35]. Tian *et al.* was able to investigate the competition between SO coupling effect and IMO interaction in a series of molecules including halogenated alkanes [36−39]. The anisotropy of an MO electron density distribution can be reflected by the slope parameters of the measured CEDPICS. However, when the IMO interactions are too weak to compete with the strong SO coupling effect, the slope parameters of CEDPICS for the SO split bands are almost equal. Thereby, the interaction anisotropy arising from the different electron distributions cannot be reflected by CEDPICS for the SO split bands.

As we have mentioned, EMS can obtain not only the ionization energies but also the electron momentum distributions for specific MOs as well [2]. From this point of view, EMS is an ideal tool to evaluate IMO interaction and SO coupling effect in low symmetry halogenated alkanes. In this work, we report the first EMS study of *n*-propyl iodide ($CH_3CH_2CH_2I$) molecule which is one of the smallest molecules undergoing IMO interaction and SO coupling simultaneously. The electron binding energies and electron momentum distributions for the outer valence orbitals are obtained. The IMO interaction and SO coupling effect are evaluated in aspects of energy as well as electron momentum distributions. One complexity that must be pointed out is that the IMO interaction is also the origin of the stereoelectronic effect that determines the conformational preferences of the molecule when the C−I group undergoes hindered internal rotations around nearby C−C single bond. The *n*-propyl iodide has been confirmed to coexist in one *trans* and two equivalent *gauche* isomers using infra-red spectra [40, 41] and microwave spectra [42]. Therefore, the thermally averaging of the two conformers needs to be taken into account in the analysis.

The ionization potentials (IPs) are calculated by using the symmetry-adapted-cluster configuration interaction (SAC-CI) general-R method [43] and relativistic density functional (DFT) method [44, 45]. It is worth noting that the SAC-CI calculation does not include the SO interaction. The relativistic and non-relativistic calculations of the theoretical electron momentum profiles (TMPs) are also carried out for the comparison with the experimental momentum profiles (XMPs).

II. EXPERIMENTAL AND THEORETICAL BACKGROUNDS

The experiment has been carried out using the non-coplanar asymmetric (e, 2e) spectrometer which has been described in detail elsewhere [46, 47]. In brief, the incident electron beam generated from an electron gun is accelerated to the energy of 2.5 keV plus the binding energy before colliding with the gas-phase molecular target injected by a nozzle. The scattered electron outgoing along polar angle θ_1=14° passes through the fast electron analyzer and is detected by a two dimensional position sensitive detector (PSD) over a large range of energies and azimuthal angles of interest. The ionized electron outgoing along polar angle θ_2=76° enters into the slow electron analyzer and is detected by a one dimension PSD.

From the conservation of energy and momentum, the binding energy ε_f and the momentum $\mathbf{p}$ of the target electron can be expressed by

$$\varepsilon_f = E_0 - E_1 - E_2 \tag{1}$$

$$\mathbf{p} = \mathbf{p}_0 - \mathbf{p}_1 - \mathbf{p}_2 \tag{2}$$

where E_i and $\mathbf{p}_i$ (i=0, 1, 2) are energies and momenta of the incident and two outgoing electrons respectively. Under the present experimental conditions, the magnitude of the momentum of the target electron can be expressed as

$$p = [{p_0}^2 + {p_1}^2 + {p_2}^2 - 2p_0p_1\cos\theta_1 - 2p_0p_2\cos\theta_2 + 2p_1p_2(\cos\theta_1\cos\theta_2 - \sin\theta_1\sin\theta_2\cos\phi)]^{1/2} \tag{3}$$

where θ_1 and θ_2 are the polar angles of the scattered and ejected electrons and ϕ is the relative azimuthal angle between the two electrons.

Within the binary encounter approximation and the plane wave impulse approximation, as well as target HF approximation or target KS approximation, the differential cross section of (e, 2e) ionization can be expressed as [2]

$$\frac{\mathrm{d}^3\sigma}{\mathrm{d}\Omega_1\mathrm{d}\Omega_2\mathrm{d}E_2} \propto S_f^i \int \mathrm{d}\Omega_p \, |\phi_i(\mathbf{p})|^2 \tag{4}$$

where $\phi_i(\mathbf{p})$ is the momentum space canonical HF or KS one-electron wavefunction of the ith orbital from which the electron is ejected. The integral in Eq.(4) is known as the spherically averaged one electron momentum distribution, or electron momentum profile.

The electron momentum distributions for the SO split components of lone pair electrons are calculated

DOI:10.1063/1674-0068/27/05/503-511

through Fourier transform and spherical integral of the position space wavefunctions calculated by relativistic DFT method. The position space SO wavefunctions can be expressed as [48]:

$$\Psi(\mathbf{r}) = \Psi_\alpha(\mathbf{r}) \cdot \alpha + \Psi_\beta(\mathbf{r}) \cdot \beta \tag{5}$$

where α and β are the spin variables which are orthogonal with each other, and $\Psi_\alpha(\mathbf{r})$ and $\Psi_\beta(\mathbf{r})$ are the relevant space wavefunctions. Through Fourier transform, we get the momentum space wavefunction,

$$\phi(\mathbf{p}) = \phi_\alpha(\mathbf{p}) \cdot \alpha + \phi_\beta(\mathbf{p}) \cdot \beta \tag{6}$$

Then, the electron momentum profile can be given by the spherically averaging of the electron momentum distribution,

$$\begin{aligned} \rho(p) &= \int \mathrm{d}\Omega_p \left|\phi(\mathbf{p})\right|^2 \\ &= \int \mathrm{d}\Omega_p \left[\left|\phi_\alpha(\mathbf{p})\right|^2 + \left|\phi_\beta(\mathbf{p})\right|^2\right] \end{aligned} \tag{7}$$

The non-relativistic TMPs for the outer valence orbitals of the two conformers of *n*-propyl iodide can be calculated according to Eq.(4), while the relativistic TMPs for the two SO split components of iodine lone pair orbitals are calculated according to Eq.(7). HF and DFT-B3LYP methods are adopted to calculate the non-relativistic electron wavefunctions with aug-cc-pVTZ basis sets for C and H and 6-311G** for I, while the relativistic wavefunctions are calculated by the relativistic DFT-B3LYP method with TZ2P basis sets, respectively.

For the sake of the comparison with the experiments, the TMPs have been folded with the angular resolutions using the Gaussian weighted planar grid methods [49]. The neutral molecular geometry and energy differences of the two conformers are optimized and calculated using the second-order Møllet-Plesset perturbation (MP2) method with aug-cc-pVTZ basis sets for C and H and 6-311G** for I. The geometrical structures of the two conformers are shown in Fig.1. The relative populations of *gauche*- and *trans*-conformers depend on the Gibbs free energy difference ΔG of the two conformers [13]. The constant K_T can be simply estimated by

$$\ln K_T = -\frac{\Delta G}{RT} \tag{8}$$

The calculated ΔG=1.33 kJ/mol corresponds to the relative abundances of 54% and 46% for *gauche*- and *trans*-conformers at room temperature.

In this work, all the non-relativistic calculations are carried out by Gaussian 09 program [50], while the relativistic calculations are performed using Amsterdam density functional 2012.01c program [44, 45].

The total energy and angular resolutions of the experimental setup are determined to be 1.0 eV (full width at half maximum (FWHM)) and $\Delta\theta\approx1^\circ$, $\Delta\phi\approx1^\circ$ respectively by measuring Ar3p ionization. The *n*-propyl iodide sample was purchased from Alfa Aesar Company with >98% purity. No impurities were observed in the spectrum.

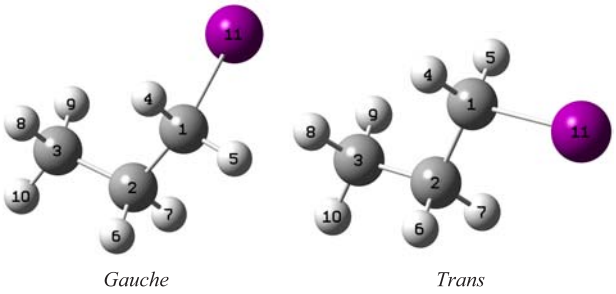

FIG. 1 Geometrical structure of *n*-propyl iodide.

III. RESULTS AND DISCUSSION

A. Binding energy spectra

The *gauche*-$CH_3CH_2CH_2I$ belongs to the C_1 point group and the *trans*-$CH_3CH_2CH_2I$ belongs to the C_s point group. The ground state electronic configurations of each conformers based on the HF calculation are:

$$\underbrace{(\mathrm{core})^{52}}_{\text{Core}}\ \underbrace{1(\mathrm{a})^2 2(\mathrm{a})^2 3(\mathrm{a})^2 4(\mathrm{a})^2}_{\text{Inner valence}}$$

$$\underbrace{5(\mathrm{a})^2 6(\mathrm{a})^2 7(\mathrm{a})^2 8(\mathrm{a})^2 9(\mathrm{a})^2 10(\mathrm{a})^2 11(\mathrm{a})^2 12(\mathrm{a})^2 13(\mathrm{a})^2}_{\text{Outer valence}}$$

for *gauche* and

$$\underbrace{(\mathrm{core})^{52}}_{\text{Core}}\ \underbrace{1(\mathrm{a}')^2 2(\mathrm{a}')^2 3(\mathrm{a}')^2 4(\mathrm{a}')^2}_{\text{Inner valence}}$$

$$\underbrace{1(\mathrm{a}'')^2 5(\mathrm{a}')^2 2(\mathrm{a}'')^2 6(\mathrm{a}')^2 7(\mathrm{a}')^2 3(\mathrm{a}'')^2 8(\mathrm{a}')^2 4(\mathrm{a}'')^2 9(\mathrm{a}')^2}_{\text{Outer valence}}$$

for *trans*.

The binding energy spectrum (BES) of *n*-propyl iodide for the outer valence orbitals is shown in Fig.2(a). Generally, four lobes are observed in the energy range of 8−18 eV. Eight Gaussian peaks are chosen to fit the BES, as shown by the dashed curves in Fig.2(a). The asymmetric Franck-Condon profiles of peak-3, 4, and 5 of PES [51] are deconvoluted by using asymmetric double Gaussian cumulative (ADGC) function [52]. The ADGC functions are then convoluted with the present instrumental energy resolution of 1.0 eV to produce the widths of peak-3, 4, and 5 of the present BES. The

DOI:10.1063/1674-0068/27/05/503-511

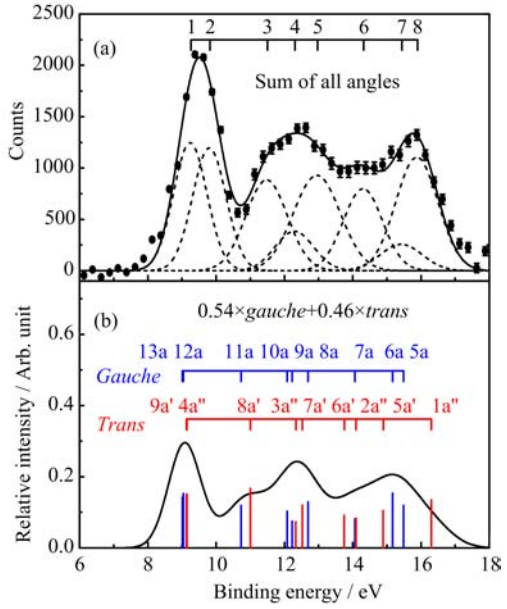

FIG. 2 (a) Binding energy spectra of *n*-propyl iodide. (b) Simulated binding energy spectra by SAC-CI general-R calculation.

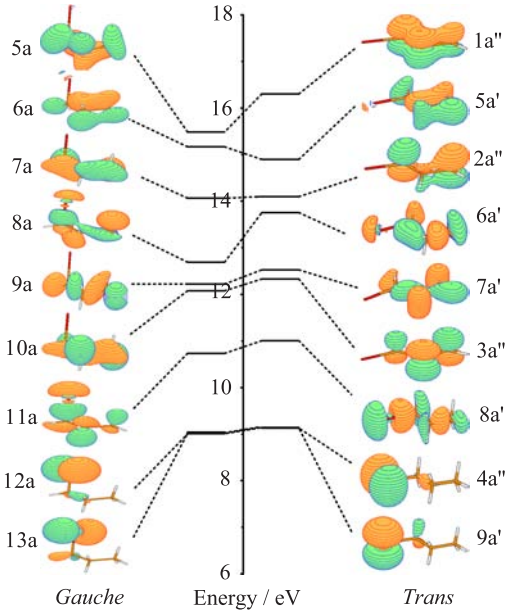

FIG. 3 The orbital correlation of the two conformers of *n*-propyl iodide. The orbital maps for the *gauche*- and *trans*-conformers are calculated by HF/aug-cc-pVTZ(C,H)6-311G** (I). The ionization potentials are calculated by SAC-CI general-R methods.

widths of the other peaks (peak-1, 2, 6, 7, 8) are determined using the present instrument function folded with the Franck-Condon widths of the PES. The positions of the Gaussian peaks are determined by the high resolution PES IPs [51]. Small adjustments have been applied to compensate the asymmetric shapes of the Franck-Condon profiles. A weak structure observed in PES [51] at 13.5 eV is not included in the present deconvolution procedure because of the low energy resolution.

The assignments of the ionization peaks are not clear in the previous PES works, except for the first two bands which can be assigned to the SO splitting of the non-bonding lone pair orbitals of iodine ($n_{\rm I}$). The coexisting of two conformers makes the assignment quite complicated. Figure 2(b) shows the simulated BES employing the IPs by SAC-CI general-R calculations convoluting with the instrumental function of 1.0 eV. The positions of the vertical bars are the calculated IPs and the heights of them represent the calculated electron intensities. Although the SAC-CI general-R methods cannot reproduce the relativistic effects of SO splitting of $n_{\rm I}$, most of the features of the BES have been reproduced by the simulation. The intensity difference is due to the inaccuracy of the SAC-CI calculations which generally underestimate the ionization potentials as shown in Table I. By comparing the experimental BES with the SAC-CI calculation, it can be seen that 9 orbitals of each *n*-propyl iodide conformers are classified into five groups: peak-1+2 for 13a+12a/9a′+4a″, peak-3 for 11a/8a′, peak-4+5 for 10a+9a+8a/3a″+7a′, peak-6 for 7a/6a′+2a″, and peak-7+8 for 6a+5a/5a′+1a″. The orbital correlation maps of the two conformers are shown in Fig.3. The results of IPs of the present EMS, SAC-CI and relativistic DFT calculations as well as previous PES are listed in Table I.

B. Comparisons of experimental and theoretical momentum profiles

The XMPs are extracted by deconvoluting the ionization peaks from the BES at different azimuthal angles ϕ and plotting the area under the corresponding fitted peak as a function of target electron momentum. The XMPs together with the corresponding thermally averaged TMPs for *gauche*- and *trans*-conformers are depicted in Fig.4. The XMPs and TMPs are area normalized by comparing the XMPs of peak-1+2 with the corresponding TMPs of HF/aug-cc-pVTZ(C,H)6-311G**(I) results.

Figure 4(a) shows the summed XMP for peak-1 and peak-2, which correspond to the SO split components of lone pair orbitals of iodine 5p (13a/9a′ and 12a/4a″). Obviously, it shows a typical "p-type" character which is in good agreement with the HF and DFT-B3LYP calculations.

Peak-3 corresponds to the ionization from the C−I bonding orbitals 11a/8a′ of the two conformers with a little bit of non-bonding iodine 4p lone pair and C−H bonding for 11a and C−C bonding for 8a′. The TMPs of individual *gauche*- and *trans*-conformers both show "sp-type" character with a second maximum at p≈1.0 a.u. as shown in Fig.4(b). The thermally averaged TMPs

DOI:10.1063/1674-0068/27/05/503-511

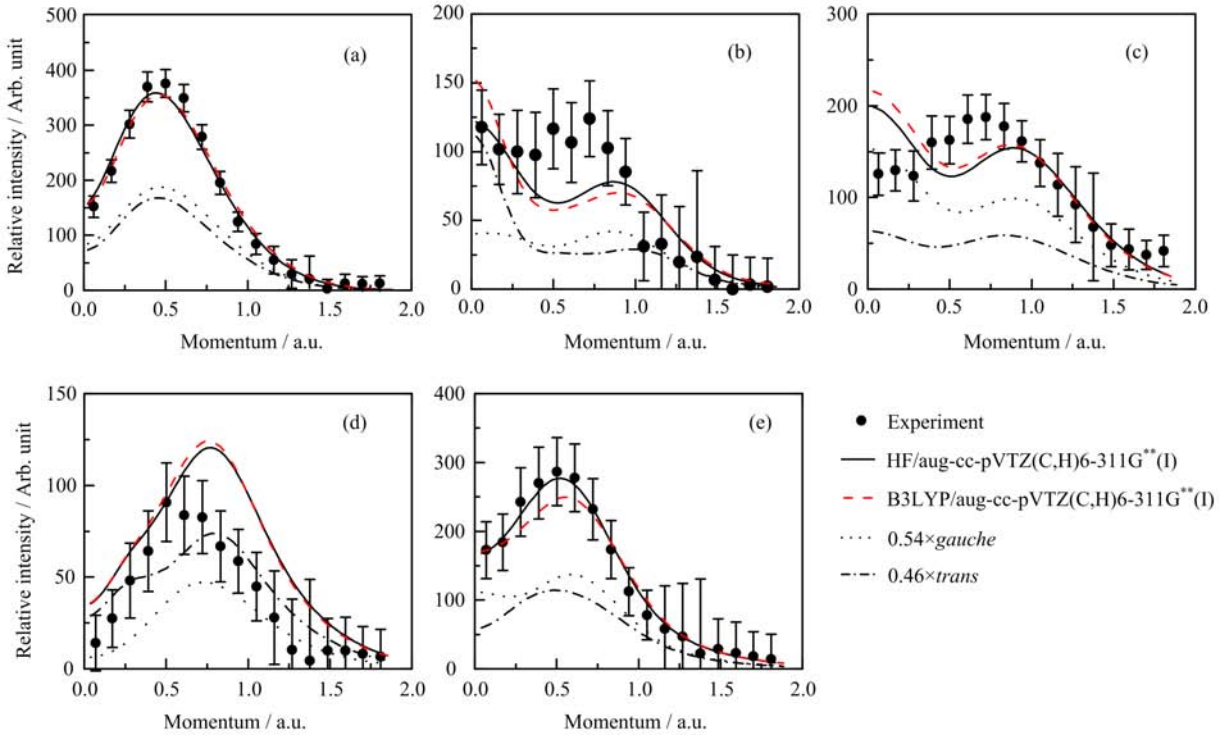

FIG. 4 The experimental and thermally averaged TMPs of the outer valence orbital of *n*-propyl iodide. (a) Peak-1+2 for 13a+12a+9a′+4a″, (b) peak-3 for 11a+8a′, (c) peak-4+5 for 10a+9a+8a+7a′+3a″, (d) peak-6 for 7a+6a′+2a″, and (e) peak-7+8 for 6a+5a+5a′+1a″.

TABLE I Ionization potential of present EMS measurement, PES results, SAC-CI general-R calculations and relativistic DFT calculations.

Peaks	Expt. IP/eV		*Gauche* (SAC-CI)			*Trans* (SAC-CI)			Relativistic DFT	
	PES[a]	EMS	IP/eV	Intensity	Config.[b]	IP/eV	Intensity	Config.[b]	*Gauche*	*Trans*
Peak-1	9.26	9.26	9.012	0.86	0.93 (13a)	9.130	0.84	0.97 (9a′)	6.55	6.57
Peak-2	9.82	9.82	9.039	0.86	0.93 (12a)	9.145	0.84	−0.97 (4a″)	7.04	7.06
Peak-3	11.38	11.50	10.732	0.85	0.97 (11a)	11.003	0.84	0.97 (8a′)	8.89	9.01
Peak-4	12.19	12.31	12.079	0.84	0.94 (10a)	12.332	0.83	−0.96 (3a″)	9.63	9.46
Peak-5	12.85	12.97	12.223	0.84	0.95 (9a)	12.525	0.83	0.96 (7a′)	9.85	9.84
S[c]	13.50		12.693	0.84	−0.94 (8a)	13.753	0.82	−0.95 (6a′)	10.27	11.12
Peak-6	14.32	14.32	14.063	0.83	−0.95 (7a)	14.098	0.82	0.95 (2a″)	11.43	11.21
Peak-7	15.44	15.44	15.166	0.83	−0.93 (6a)	14.893	0.83	−0.96 (5a′)	12.56	11.92
Peak-8	15.90	15.90	15.487	0.82	−0.93 (5a)	16.300	0.81	0.95 (1a″)	12.80	13.19

[a] High resolution photoelectron spectroscopy from Ref.[51].
[b] Main configuration ($|C|>0.3$).
[c] Weak structure identified in PES [51].

are consistent with the XMPs in shape but underestimate the intensity between 0.4 and 0.9 a.u. Such phenomenon may be ascribed to the ultrafast motion of the atoms during the ionization. While the C−I bonds are broken on the kicking out of the relevant orbital electron, the molecule will dissociate. Estimated from the potential energy curve of the reaction paths [53], the time for the C−I bond extending from stable geometry (2.12 Å for *gauche*- and 2.11 Å for *trans*-conformer) to 2.50 Å is about several femtosecond, which is comparable to the collision time of the electron impact reaction. The TMPs at different C−I lengths of neutral *n*-propyl iodide are calculated using HF/aug-cc-pVTZ(C,H)6-311G**(I). As is expected, the intensities in the middle momentum region arise with the extension of the C−I bonds while the intensities reduce in the low momentum region, as shown in Fig.5(a), indicating the possible ultrafast nuclear motion.

DOI:10.1063/1674-0068/27/05/503-511

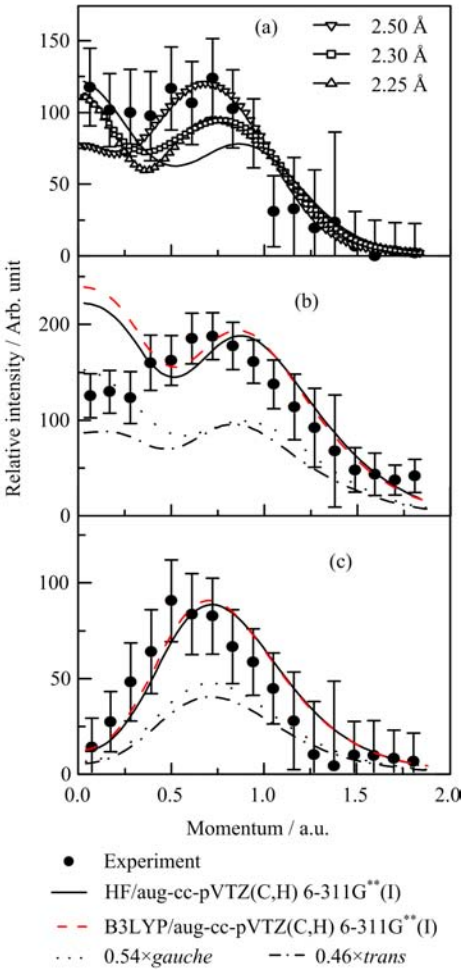

FIG. 5 (a) TMPs comparing with XMPs for thermally averaged TMPs of peak-3 for 11a+8a′ at different C−I bond length. The solid line indicates the thermally averaged TMPs of the stable geometry. (b) TMPs of peak-4 for 10a+9a+8a of *gauche*-conformer and 3a″+7a′+6a′ of *trans*-conformer together with XMPs of peak-4+5. (c) TMPs of peak-6 for 7a+2a″ comparing with XMPs of peak-6.

The comparisons of TMPs and XMPs for peak-4+5 (10a+9a+8a++7a′3a″) and peak-6 (7a+6a′+2a″) are shown in Fig.4 (c) and (d). The TMPs for peak-4+5 underestimate the intensity of the XMPs in the middle momentum region while the TMPs for peak-6 overestimate the intensity over the whole momentum range. Such disagreements may result from the ascription of 6a′ orbital. The results of the SAC-CI calculation indicate that 6a′ orbital of the *trans*-conformer is very close to the 2a″ orbital as comparing 8a to 7a of the *gauche*-conformer. The calculation may overestimate the ionization potential of 6a′ of the *trans*-conformer. To testify this possibility, the TMP of 6a′ is included in peak-4+5. As shown in Fig.5 (b) and (c), the agreement between TMPs and XMPs for peak-4+5 and peak-6 has significantly been improved, except the low momentum region for peak-4+5. The reason of the discrepancy remains unclear.

For the last lobe in BES, peak-7+8, which corresponds to C−C and C−H bonding orbitals of 6a+5a/5a′+1a″, the XMP shows a "p-type" character (Fig.4(e)). Both HF and DFTB3LYP/aug-cc-pVTZ(C,H)6-311G**(I) calculations well reproduce the experiment.

C. Evaluation of spin-orbit coupling effect and intramolecular orbital interaction

SO coupling and IMO interaction may co-exist in *n*-propyl iodide. As can be seen in Table I, the non-relativistic calculation of SAC-CI general-R predicts that the energy difference between peak-1 (13a/9a′) and peak-2 (12a/4a″) is 0.027 eV for *gauche*-conformer and 0.015 eV for *trans*-conformer, which is much smaller than the experimental result (0.56 eV). On the other hand, the relativistic DFT/TZ2P calculation predicts the IPs of the first two bands to be 6.55 and 7.04 eV for *gauche*-conformer and 6.57 and 7.06 eV for *trans*-conformer. The energy difference is 0.49 eV, which is comparable to the experimental observation (0.56 eV). Note that the SAC-CI general-R calculation implies the consideration of IMO interactions but does not include SO coupling. The result indicates that the IMO interactions between iodine 5p lone pairs and other moieties of *n*-propyl iodide molecule will not lead to an observed energy difference for the first two bands. However, this does not necessarily mean the absence of the IMO interactions. As can be seen in the orbital maps in Fig.3, for the HOMOs 13a/9a′ and next HOMOs 12a/4a″, the delocalization of electron density distribution of $n_{\rm I}$ is obvious, which is the result of the hyperconjugative interaction [8, 28, 29].

Natural bond orbital (NBO) theory [54, 55] has been extensively used to analyze the IMO interactions. NBO analysis transforms the canonical delocalized MOs into the localized orbitals, and the hyperconjugative interaction can be treated by

$$E(2) = -\frac{n_\sigma F_{ij}^2}{\Delta\varepsilon} \tag{9}$$

where F_{ij} is the Fock matrix between the unperturbed occupied σ and unoccupied antibonding σ^* natural orbitals, n_σ is the σ population, and $\Delta\varepsilon$ is the energy difference between the unperturbed σ and σ^* orbitals. The NBO analyses are performed with NBO 5.9 program [55]. The results are listed in Table II. The $n_{\rm I}\rightarrow\sigma^*$ interactions lead to the lowered energy levels of the occupied orbitals. The energy lowering due to these delocalization interactions can be approximated by the sum of the $E(2)$ energies. For HOMO ($n_{\rm I}^{\perp}$) and next HOMO ($n_{\rm I}^{\parallel}$) of *gauche*-conformer, the energy levels are lowered by ∼0.250 and ∼0.271 eV respectively. While for *trans*-conformer, the energy declines of HOMO ($n_{\rm I}^{\perp}$)

DOI:10.1063/1674-0068/27/05/503-511

TABLE II The NBO analyses of *gauche*- and *trans*-conformers of *n*-propyl iodide.

Donor[a]	*Gauche*		*Trans*	
	Acceptor	$E(2)$[b]	Acceptor	$E(2)$[b]
$n_{\mathrm{I}}^{\perp}$	$\sigma^*_{\mathrm{C1-H4}}$	3.58	$\sigma^*_{\mathrm{C1-H4}}$	3.09
	$\sigma^*_{\mathrm{C1-H5}}$	2.19	$\sigma^*_{\mathrm{C1-H5}}$	3.09
$n_{\mathrm{I}}^{\parallel}$	$\sigma^*_{\mathrm{C1-C2}}$	3.41	$\sigma^*_{\mathrm{C1-C2}}$	3.22
	$\sigma^*_{\mathrm{C3-H9}}$	0.51	$\sigma^*_{\mathrm{C1-H4}}$	0.91
	$\sigma^*_{\mathrm{C1-H5}}$	1.47	$\sigma^*_{\mathrm{C1-H5}}$	0.91
	$\sigma^*_{\mathrm{C2-H6}}$	0.86	$\sigma^*_{\mathrm{C2-C3}}$	1.19

[a] $n_{\mathrm{I}}^{\perp}$ and $n_{\mathrm{I}}^{\parallel}$ refer to the unperturbed 5p lone pair orbitals of iodine atom. σ^* represent unoccupied anti-bonding orbitals.
[b] $E(2)$ is in kcal/mol. The values smaller than 0.5 kcal/mol are omitted.

and next HOMO ($n_{\mathrm{I}}^{\parallel}$) are estimated to be ∼0.268 and ∼0.270 eV. These will lead to energy differences of 0.021 and 0.002 eV for *gauche*- and *trans*-conformers, which are consistent with the non-relativistic calculations.

On the other hand, the hyperconjugative interactions will lead to the delocalization of the iodine 5p lone pairs of HOMO and next HOMO for both *gauche*- and *trans*-conformers and result in an observed difference in electron density distributions. In both conformers, two predominant $n_{\mathrm{I}}\rightarrow\sigma^*_{\mathrm{CH}}$ interactions lead to the two delocalized components $\sigma_{\mathrm{C1-H4}}$ and $\sigma_{\mathrm{C1-H5}}$ of HOMO, while the predominant $n_{\mathrm{I}}\rightarrow\sigma^*_{\mathrm{CC}}$ interaction leads to the delocalized component $\sigma_{\mathrm{C1-C2}}$ of next HOMO. The non-relativistic calculated TMPs by B3LPY/aug-cc-pVTZ(C,H)6-311G**(I) for HOMO (13a) and next HOMO (12a) of *gauche*-conformer, and TMPs for HOMO (9a′) and next HOMO (4a″) of *trans*-conformer are shown in Fig.6 (a) and (b). It can be seen that, including IMO interactions, the non-relativistic TMPs show distinct difference, having lower intensity for HOMO than for next HOMO in the momentum region p<0.5 a.u. As shown in our previous work in CF_3I [20], the different SO split components of n_{I} also exhibit different momentum distributions due to the relativistic effect. The intensity of momentum distribution for large j component (HOMO: $^2E_{3/2}$) in low momentum region is larger than that for small j component (next HOMO: $^2E_{1/2}$) and the case is inversed in high momentum region. The same situation can be observed in the relativistic calculated TMPs by DFT/TZ2P in Fig.6 (c) and (d).

In order to compare the XMPs with the TMPs for HOMO and next HOMO, we plot individual XMPs of peak-1 and peak-2 in Fig.6(e) together with the thermally averaged relativistic TMPs. Although the uncertainties are pretty large, it is obvious that intensity of XMP for HOMO ($^2E_{3/2}$) in low momentum region is larger than that for next HOMO ($^2E_{1/2}$),

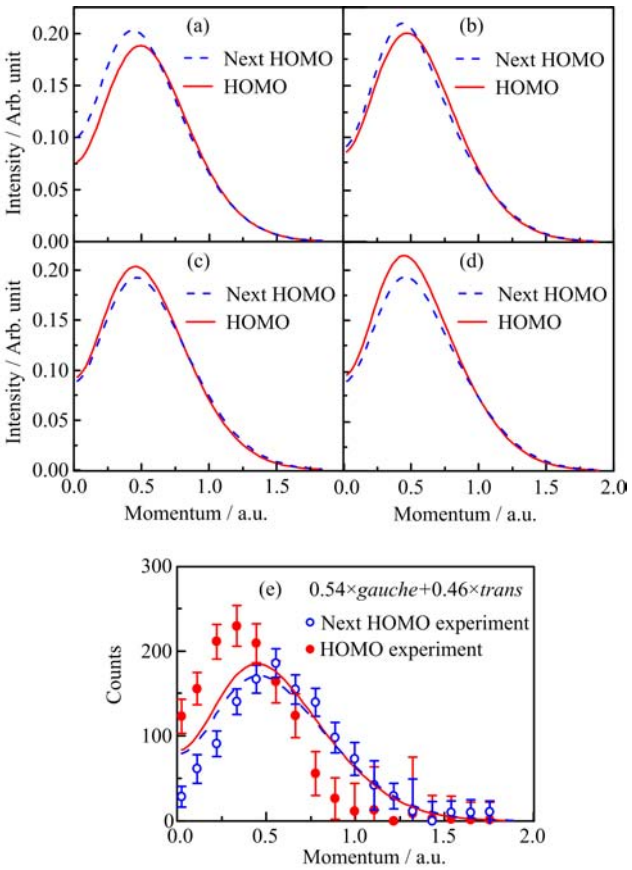

FIG. 6 The TMPs and XMPs for HOMO and next HOMO. Non-relativistic calculated TMPs for (a) *gauche*-conformer and (b) *trans*-conformer by B3LPY/aug-cc-pVTZ(C,H)6-311G**(I). Relativistic calculated TMPs for (c) *gauche*-conformer and (d) relativistic TMPs for *trans*-conformer by DFT/TZ2P. (e) Thermally averaged TMPs of *gauche*-conformer and *trans*-conformer together with the XMPs (solid line is HOMO relativistic calculated TMPs by DFT/TZ2P, dash line is next HOMO relativistic calculated TMPs by DFT/TZ2P).

indicating that the SO coupling effect dominates in the first two bands of *n*-propyl iodide.

IV. CONCLUSION

In this work, we have reported the first EMS measurements on the outer valence orbitals of *n*-propyl iodide. The binding energy spectrum and electron momentum distributions have been obtained. The results are interpreted by both non-relativistic and relativistic calculations taking into account the relative abundance of 54% for *gauche*- and 46% for *trans*-conformers. The ionization peaks have been assigned in detail by the comparison between the experimental BES and the simulated BES using the results of calculation by the high accuracy SAC-CI general-R method. The XMPs are compared with the TMPs calculated by HF and

DOI:10.1063/1674-0068/27/05/503-511

B3LYP/aug-cc-pVTZ(C,H)6-311G**(I). The XMPs for the first two bands have been extracted and compared with non-relativistic and relativistic calculations. Both NBO analysis and non-relativistic calculated TMPs show that IMO interactions play roles in HOMO and next HOMO of *n*-propyl iodide, which are iodine lone pair orbitals, and lead to an observed difference in TMPs. On the other hand, the relativistic calculations show that the SO coupling effect leads to the splitting of the first two bands. The relativistic effect will also result in an observed difference in TMPs. It is found that SO coupling effect and IMO interaction lead to opposite trends in the change of electron momentum distributions. The experimental results agree with the relativistic TMPs, indicating that the SO coupling effect dominates in *n*-propyl iodide.

V. ACKNOWLEDGMENTS

This work was supported by the National Basic Research Program of China (No.2010CB923301), the National Natural Science Foundation of China (No.11327404, No.20973160, and No.10904136), and the Fundamental Research Funds for the Central Universities. The SAC-CI calculations have been done on the supercomputing system in the Supercomputing Center of University of Science and Technology of China.

[1] I. E. McCarthy and E. Weigold, Rep. Prog. Phys. **54**, 789 (1991).
[2] E. Weigold and I. E. McCarthy, *Electron Momentum Spectroscopy*, New York: Kluwer Academic/Plenum Press, (1999).
[3] C. E. Brion, Int. J. Quantum Chem. **29**, 1397 (1986).
[4] M. A. Coplan, J. H. Moore, and J. P. Doering, Rev. Mod. Phys. **66**, 985 (1994).
[5] P. Duffy, D. P. Chong, M. E. Casida, and D. R. Salahub, Phys. Rev. A **50**, 4707 (1994).
[6] M. Takahashi, M. Matsuo, and Y. Udagawa, Chem. Phys. Lett. **308**, 195 (1999).
[7] M. Takahashi, R. Ogino, and Y. Udagawa, Chem. Phys. Lett. **288**, 714 (1998).
[8] X. J. Chen, F.Wu, M. Yan, H. B. Li, S. X. Tian, X. Shan, K. D. Wang, Z. J. Li, and K. Z. Xu, Chem. Phys. Lett. **472**, 19 (2009).
[9] Y. Zheng, J. J. Neville, and C. E. Brion, Science **270**, 786 (1995).
[10] M. S. Deleuze, W. N. Pang, A. Salam, and R. C. Shang, J. Am. Chem. Soc. **123**, 4049 (2001).
[11] M. S. Deleuze and S. Knippenberg, J. Chem. Phys. **125**, 104309 (2006).
[12] Y. R. Huang, S. Knippenberg, B. Hajgató, J. P. François, J. K. Deng, and M. S. Deleuze, J. Phys. Chem. A **111**, 5879 (2007).
[13] F. Wu, X. J. Chen, X. Shan, S. X. Tian, Z. J. Li, and K. Z. Xu, J. Phys. Chem. A **112**, 4360 (2008).
[14] C. G. Ning, Y. R. Huang, S. F. Zhang, J. K. Deng, K. Liu, Z. H. Luo, and F. Wang, J. Phys. Chem. A **112**, 1078 (2008).
[15] X. X. Xue, M. Yan, F. Wu, X. Shan, K. Z. Xu, and X. J. Chen, Chin. J. Chem. Phys. **21**, 515 (2008).
[16] C. G. Ning, Z. H. Luo, Y. R. Huang, B. Hajgató, F. Morini, K. Liu, S. F. Zhang, J. K. Deng, and M. S. Deleuze, J. Phys. B **41**, 175103 (2008).
[17] M. Yan, X. Shan, F. Wu, X. X. Xia, K. D. Wang, K. Z. Xu, and X. J. Chen, J. Phys. Chem. A **113**, 507 (2009).
[18] J. P. D. Cook, J. Mitroy, and E. Weigold, Phys. Rev. Lett. **52**, 1116 (1984).
[19] X. G. Ren, C. G. Ning, J. K. Deng, G. L. Su, S. F. Zhang, and Y. R. Huang, Phys. Rev. A **73**, 042714 (2006).
[20] Z. J. Li, X. J. Chen, X. Shan, X. X. Xue, T. Liu, and K. Z. Xu, Chem. Phys. Lett. **457**, 45 (2008).
[21] K. Liu, C. G. Ning, and J. K. Deng, Phys. Rev. A **80**, 022716 (2009).
[22] J. S. Zhu, J. K. Deng, and C. G. Ning, Phys. Rev. A **85**, 052714 (2012).
[23] J. Doucet, P. Sauvageau, and C. Sandorfy, J. Chem. Phys. **58**, 3708 (1973).
[24] K. Kimura, S. Katsumata, Y. Achiba, H. Matsumoto, and S. Nagakura, Bull. Chem. Soc. Jpn. **46**, 373 (1973).
[25] I. Novak, D. B. Li, A. W. Potts, A. Shareef, and B. Kovač, J. Org. Chem. **67**, 3510 (2002).
[26] F. Brogli and E. Heilbronner, Helv. Chim. Acta **54**, 1423 (1971).
[27] I. Grant, *Relativistic Quantum Theory of Atoms and Molecules Theory and Computation*, New York: Springer, (2007).
[28] R. S. Mulliken, J. Chem. Phys. **7**, 339 (1939).
[29] R. S. Mulliken, C. A. Rieke, and W. G. Brown, J. Am. Chem. Soc. **63**, 41 (1941).
[30] F. Penning, Naturwissenschaften **15**, 818 (1927).
[31] K. Ohno, H. Mutoh, and Y. Harada, J. Am. Chem. Soc. **105**, 4555 (1983).
[32] K. Ohno, S. Matsumoto, and Y. Harada, J. Chem. Phys. **81**, 4447 (1984).
[33] K. Mitsuke, T. Takami, and K. Ohno, J. Chem. Phys. **91**, 1618 (1989).
[34] K. Ohno, T. Takami, K. Mitsuke, and T. Ishida, J. Chem. Phys. **94**, 2675 (1991).
[35] T. Takami, K. Mitsuke, and K. Ohno, J. Chem. Phys. **95**, 918 (1991).
[36] S. X. Tian, N. Kishimoto, and K. Ohno, J. Electron Spectrosc. Relat. Phenom. **125**, 205 (2002).
[37] S. X. Tian, N. Kishimoto, and K. Ohno, J. Phys. Chem. A **106**, 7714 (2002).
[38] S. X. Tian, N. Kishimoto, and K. Ohno, J. Phys. Chem. A **107**, 485 (2003).
[39] S. X. Tian, N. Kishimoto, and K. Ohno, J. Phys. Chem. A **107**, 2137 (2003).
[40] J. K. Brown and N. Sheppard, Trans. Faraday Soc. **50**, 1164 (1954).
[41] K. Radcliffe and J. L. Wood, Trans. Faraday Soc. **62**, 1678 (1966).
[42] Y. Niide, I. Ohkoshi, and M. Takano, J. Mol. Spectrosc. **122**, 113 (1987).
[43] H. Nakatsuji and K. Hirao, J. Chem. Phys. **68**, 2053 (1978).
[44] C. Fonseca Guerra, J. G. Snijders, G. te Velde, and E.

J. Baerends, Theor. Chem. Acc. **99**, 391 (1998).
[45] G. te Velde, F. M. Bickelhaupt, E. J. Baerends, C. Fonseca Guerra, S. J. A. van Gisbergen, J. G. Snijders, and T. Ziegler, J. Comput. Chem. **22**, 931 (2001).
[46] X. Shan, X. J. Chen, L. X. Zhou, Z. J. Li, T. Liu, X. X. Xue, and K. Z. Xu, J. Chem. Phys. **125**, 154307 (2006).
[47] X. J. Chen, X. Shan, and K. Z. Xu, *in Nanoscale Interactions and Their Applications: Essays in Honour of Ian McCarthy*, Kerala: Transworld Research Network, 37 (2007).
[48] K. Liu, C. G. Ning, and J. K. Deng, Chin. Phys. Lett. **27**, 073403 (2010).
[49] P. Duffy, M. E. Cassida, C. Brion, and D. Chong, Chem. Phys. **159**, 347 (1992).
[50] M. J. Frisch, G. W. Trucks, H. B. Schlegel, G. E. Scuseria, M. A. Robb, J. R. Cheeseman, G. Scalmani, V. Barone, B. Mennucci, G. A. Petersson, H. Nakatsuji, M. Caricato, X. Li, H. P. Hratchian, A. F. Izmaylov, J. Bloino, G. Zheng, J. L. Sonnenb erg, M. Hada, M. Ehara, K. Toyota, R. Fukuda, J. Hasegawa, M. Ishida, T. Naka jima, Y. Honda, O. Kitao, H. Nakai, T. Vreven, J. A. Jr. Montgomery, J. E. Peralta, F. Ogliaro, M. Bearpark, J. J. Heyd, E. Brothers, K. N. Kudin, V. N. Staroverov, R. Kobayashi, J. Normand, K. Raghavachari, A. Rendell, J. C. Burant, S. S. Iyengar, J. Tomasi, M. Cossi, N. Rega, J. M. Millam, M. Klene, J. E. Knox, J. B. Cross, V. Bakken, C. Adamo, J. Jaramillo, R. Gomp erts, R. E. Stratmann, O. Yazyev, A. J. Austin, R. Cammi, C. Pomelli, J. W. Ochterski, R. L. Martin, K. Morokuma, V. G. Zakrzewski, G. A. Voth, P. Salvador, J. J. Dannenb erg, S. Dapprich, A. D. Daniels, Ö. Farkas, J. B. Foresman, J. V. Ortiz, J. Cioslowski, and D. J. Fox, *Gaussian 09*, Wallingford CT: Gaussian Inc., (2009).
[51] K. Kimura, S. Katsumata, Y. Achiba, T. Yamazaki, and S. Iwata, *Handbook of HeI Photoelectron Spectra of Fundamental Organic molecules*, Tokyo: Japan Scientific Societies Press, 87 (1981).
[52] Z. J. Li, X. J. Chen, X. Shan, T. Liu, and K. Z. Xu, J. Chem. Phys. **130**, 054302 (2009).
[53] S. T. Park, S. K. Kim, and M. S. Kim, Nature **415**, 306 (2002).
[54] A. E. Reed, L. A. Curtiss, and F. Weinhold, Chem. Rev. **88**, 899 (1988).
[55] E. Glendening, J. Badenhoop, A. Reed, J. Carpenter, and F. Weinhold, *NBO 5.9, Madison*, WI: Theoretical Chemistry Institute, University of Wisconsin, (1996).

DOI:10.1063/1674-0068/27/05/503-511